

Binding of the Amphetamine-like 1-Phenyl-piperazine to Monoamine Transporters

Kasper Severinsen,[†] Johan F. Kraft,[‡] Heidi Koldsgaard,[‡] Katrine A. Vinberg,[†] Richard B. Rothman,[§][⊥], John S. Partilla,[⊥] Ove Wiborg,[†] Bruce Blough,[§] Birgit Schiøtt,^{*,‡} and Steffen Sinning^{*,†}

[†]Laboratory of Molecular Neurobiology, Centre for Psychiatric Research, Aarhus University Hospital, Risskov, Denmark

[‡]Center for Insoluble Protein Structures (*inSPIN*), Interdisciplinary Nanoscience Center (*iNANO*), Department of Chemistry, Aarhus University, Langelandsgade 140, DK-8000 Aarhus C, Denmark

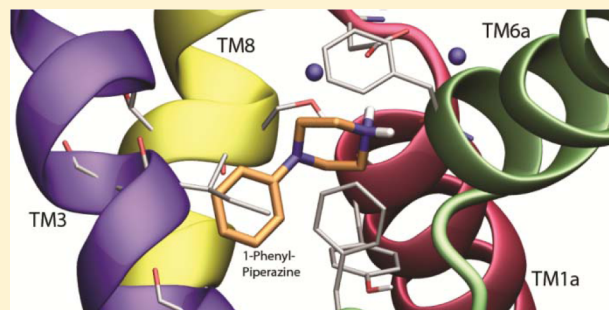
[§]Center for Organic and Medicinal Chemistry, Research Triangle Institute, Research Triangle Park, North Carolina, United States

[⊥]Translational Pharmacology Section, Intramural Research Program, National Institute on Drug Abuse, National Institutes of Health, Baltimore, Maryland 21224, United States

Supporting Information

ABSTRACT: The human serotonin transporter (hSERT), the human dopamine transporter (hDAT), and the human norepinephrine transporter (hNET) facilitate the active uptake of the neurotransmitters serotonin, dopamine, and norepinephrine from the synaptic cleft. Drugs of abuse such as MDMA (streetname “ecstasy”) and certain 1-phenyl-piperazine (PP) analogs such as 1-(3-chlorophenyl)-piperazine (mCPP) elicit their stimulatory effect by elevating the synaptic concentration of serotonin by blocking or reversing the normal transport activity of hSERT. Recent data suggest that certain analogs of PP may be able to counteract the addictive effect of cocaine. Little is still known about the precise mechanism by which MDMA and PP analogs function at hSERT, hDAT, and hNET and even less is known about the specific protein–ligand interactions. In this study, we provide a comprehensive biochemical examination of a repertoire of PP analogs in hSERT, hDAT, and hNET. Combined with induced fit docking models and molecular dynamics simulations of PP and 1-(3-hydroxyphenyl)-piperazine (3-OH-PP) bound to hSERT and hDAT, we present detailed molecular insight into the promiscuous binding of PP analogs in the monoamine transporters. We find that PP analogs inhibit uptake as well as induce release in all three monoamine transporters. We also find that the selectivity of the PP analogs can be adjusted by carefully selecting substituents on the PP skeleton.

KEYWORDS: Dopamine transporter, serotonin transporter, induced fit docking, phenyl-piperazine, cocaine, LeuT



Monoaminergic neurotransmission in the central nervous system uses the monoamines (MAs), norepinephrine (NE), dopamine (DA), and serotonin (5-HT), to convert the electrical nerve impulse into a chemical signal capable of crossing the synaptic junction. The monoamine transporters facilitate the active uptake of MAs from the synaptic cleft thereby modulating the concentration of the neurotransmitter available to stimulate the receptors on the postsynaptic neuron. Deficits in the regulation of the synaptic concentration of MAs are coupled to a broad repertoire of psychiatric disorders, for example, anorexia, obsessive-compulsive disorder, anxiety, and depression; hence many modern psychopharmacotherapies target these transporters.¹ In addition, several drugs of abuse such as cocaine and 3,4-methylenedioxymethamphetamine (MDMA; streetname, ecstasy) target the monoamine transporters and elicit their stimulatory effects by inhibiting or reversing normal transport activity.^{2–4} Inhibitors with abuse potential are often characterized by rapid brain accumulation and dopamine transporter inhibition causing elevated DA levels

in the mesolimbic reward circuit.^{5–8} Releaser type stimulants such as amphetamine and MDMA also flood the synapse with MAs by not solely relying on endogenous tone but also causing the monoamine transporters to efflux neurotransmitter.

As a natural consequence of the enormous socio-economic burden caused by the variety of MA-correlated diseases, the monoamine transporters have been subjected to extensive investigations. It has become increasingly clear that this class of transporters is very complex with regard to both transport mechanism and derived psychopharmacology. Especially, the mechanisms by which the so-called monoamine releasers, for example, MDMA, phenyl-piperazine (PP), and some PP analogs as 1-(3-chlorophenyl)-piperazine (mCPP) and 1-(3-trifluoromethylphenyl)-piperazine (TFMPP or “Legal X”) reverse the direction of the normal transport pathway of 5-

Received: April 13, 2012

Accepted: June 10, 2012

Published: June 10, 2012



HT, thereby causing efflux, are not well understood. While the inhibitor cocaine, which is similar to certain antidepressants,⁹ relies on endogenous tone by inhibiting the uptake of already released neurotransmitter by the monoamine transporters, the releasers are substrates of the monoamine transporters. The releasers thereby both compete for the uptake site with neurotransmitter and also cause efflux of the neurotransmitter through the transporter. These effects converge to an increase in the extracellular concentration of monoamine neurotransmitters.

Accumulating evidence suggests that the design of novel addiction pharmacotherapies may utilize the agonist-substitution therapy paradigm; in this context, releasers that selectively target hDAT and hSERT and leave hNET untouched have the potential for being applied in cocaine addiction pharmacotherapies. It is expected that the structure of new addiction pharmacotherapies are either variations of existing drugs of abuse with characteristics giving them slower onset of action and prolonged duration of action or variations of existing drugs of abuse with attributes giving them different selectivity for the different monoamine transporters.^{10–13} In concert with this idea, we aim at gaining structural insight on how PP analogs bind to hSERT, hDAT, and hNET.

In recent years, small molecules belonging to the PP class have attracted some attention in the development of new multiple action drugs targeting more than one protein, which can be applied in the treatment of different psychiatric illnesses. For instance, drug leads belonging to the PP series of compounds that are both NET inhibitors and 5-HT_{1A} receptor partial agonists have been identified for potential treatment of attention deficit hyperactivity disorder.¹⁴ Fine-tuning of the substituents on the PP skeleton gave a new class of triple action drugs from the bis-aryl-sulfanyl amine class of compounds that has been taken to late clinical phases for the treatment of mood disorder and anxiety. These drugs function as 5-HT enhancers, so-called 5-HT modulator and stimulators, which possess hSERT inhibitory characteristics as well as 5-HT_{3A} receptor antagonist and 5-HT_{1A} receptor partial agonist activity.¹⁵

Understanding the selectivity and mechanism of the MA releasers will aid the rational design of novel addiction pharmacotherapies. However, this necessitates a detailed knowledge of not only the molecular transport mechanism but also the specific protein–ligand interactions that precede the release of substrate to the extracellular space. The principal aim of this study is to provide a detailed picture of how the MA releasers from the PP class orient and bind inside the substrate binding pocket of the monoamine transporters.

We employed induced fit docking (IFD) of PP and 3-OH-PP in both hSERT and hDAT homology models to obtain a repertoire of likely orientations of PP compounds within the binding site. The proposed binding modes were then challenged by experimental investigations in a comprehensive paired mutant–ligand analog complementation (PaMLAC) series of experiments^{16–18} yielding inhibitory potencies for 20 PP analogs in wild-type (wt) and 8 different hSERT mutant constructs. Molecular dynamics (MD) simulations of PP and 3-OH-PP were performed to assess the dynamics of the ligands in the proposed binding modes and the stability of the proteins. Finally, the selectivity of the PP analogs toward hSERT, hDAT, and hNET were examined using eight PP analogs in uptake experiments. A broader repertoire of 24 PP analogs was applied in release experiments. All PP analogs employed in the study are displayed in Chart 1.

Chart 1. Chemical Structures of PP Analogs Employed

	R ₂	R ₃	R _{3'}	R ₄
PP	-H	-H	-H	-H
2-Me-PP	-CH ₃	-H	-H	-H
2-Et-PP	-CH ₂ CH ₃	-H	-H	-H
2-SMe-PP	-SCH ₃	-H	-H	-H
2-OEt-PP	-OCH ₂ CH ₃	-H	-H	-H
2-CN-PP	-CN	-H	-H	-H
2-CF ₃ -PP	-CF ₃	-H	-H	-H
2-nitro-PP	-NO ₂	-H	-H	-H
2-chloro-PP	-Cl	-H	-H	-H
2-bromo-PP	-Br	-H	-H	-H
3-Me-PP	-H	-CH ₃	-H	-H
3-OMe-PP	-H	-OCH ₃	-H	-H
3-OH-PP	-H	-OH	-H	-H
3-fluoro-PP	-H	-H	-F	-H
4-Me-PP	-H	-H	-H	-CH ₃
4-Ac-PP	-H	-H	-H	-COCH ₃
4-CN-PP	-H	-H	-H	-CN
4-OH-PP	-H	-H	-H	-OH
4-nitro-PP	-H	-H	-H	-NO ₂
4-fluoro-PP	-H	-H	-H	-F
4-phenyl-PP	-H	-H	-H	-C ₆ H ₅
2,3-dichloro-PP	-Cl	-Cl	-H	-H
2,3-diMe-PP	-CH ₃	-CH ₃	-H	-H
2,4-difluoro-PP	-F	-H	-H	-F
3,4-difluoro-PP	-H	-F	-H	-F
3,3'-diOMe-PP	-H	-OCH ₃	-OCH ₃	-H
3,3'-Me ₂ OH-PP	-H	-CH ₃	-OH	-H
3,3'-OMe,OH-PP	-H	-OCH ₃	-OH	-H
3,3'-diOH-PP	-H	-OH	-OH	-H

RESULTS AND DISCUSSION

Computational Results. Molecular Docking and Cluster Analysis. IFD calculations were performed to establish models of the binding of PP and 3-OH-PP in hSERT. To fully explore the conformational freedom of the piperazine moiety, four conformations of this ring were used, namely, twist boat (T) or chair (C) conformations of the six-membered cyclic ring. These ring conformations were combined with either axial (A) or equatorial (E) positioning of the phenyl substituent located at N1 (Chart 1). The four conformations of PP, referred to as CA (chair–axial), CE (chair–equatorial), TA (twist boat–axial), and TE (twist boat–equatorial), were all used as input structures of the ligand in the docking calculations in hSERT. The IFD calculations of PP in hSERT resulted in a total of 67 poses, while IFD calculation of 3-OH-PP in hSERT resulted in a total of 60 poses, see Table 1.

Average glide docking scores (GlideScore) and E-model scores for the different clusters are listed in Table 1. Please see the Methods section for a description of the individual scores. All data for the returned poses is included in the Supporting Information. The PP poses were subjected to a cluster analysis using the XCluster facility^{19,20} in the Schrödinger software package. Clustering was performed based on the position and orientation of the phenyl ring, because the piperazine ring of the ligands did not show any distinctly preferred orientation, see Figure 1a. The method and the detailed output from the XCluster analysis are provided in the Supporting Information. From the cluster analysis, the minimum separation ratio was found to be very close to unity for all clustering levels. This indicates that there was no significant structural difference among any clusters generated of PP and that the different poses all belong to the same binding motif. However, a tendency for four small subclusters could be identified by visual inspection of

Table 1. The Results of the IFD Calculations are shown for PP and 3-OH-PP with computed Standard Deviations Included in the Supporting Information^a

	total number of poses	average prime energy (kcal/mol)	average IFDScore (kcal/mol)	average GlideScore (kcal/mol)	average E-model (kcal/mol)
PP					
outliers	24	-19031.1	-960.7	-9.1	-43.6
PP cluster 1	18	-19039.9	-961.3	-9.3	-46.1
PP cluster 2	9	-19029.0	-960.9	-9.5	-49.6
PP cluster 3	9	-19050.7	-961.2	-8.7	-57.6
PP cluster 4	7	-19028.0	-961.7	-10.3	-51.1
3-OH-PP					
cluster 1 (3-OH cluster 1)	16	-19065.8	-962.2	-8.9	-53.7
cluster 2 (3-OH cluster 2)	43	-19077.0	-963.2	-9.3	-52.6

^aStandard deviations are included in the Supporting Information.

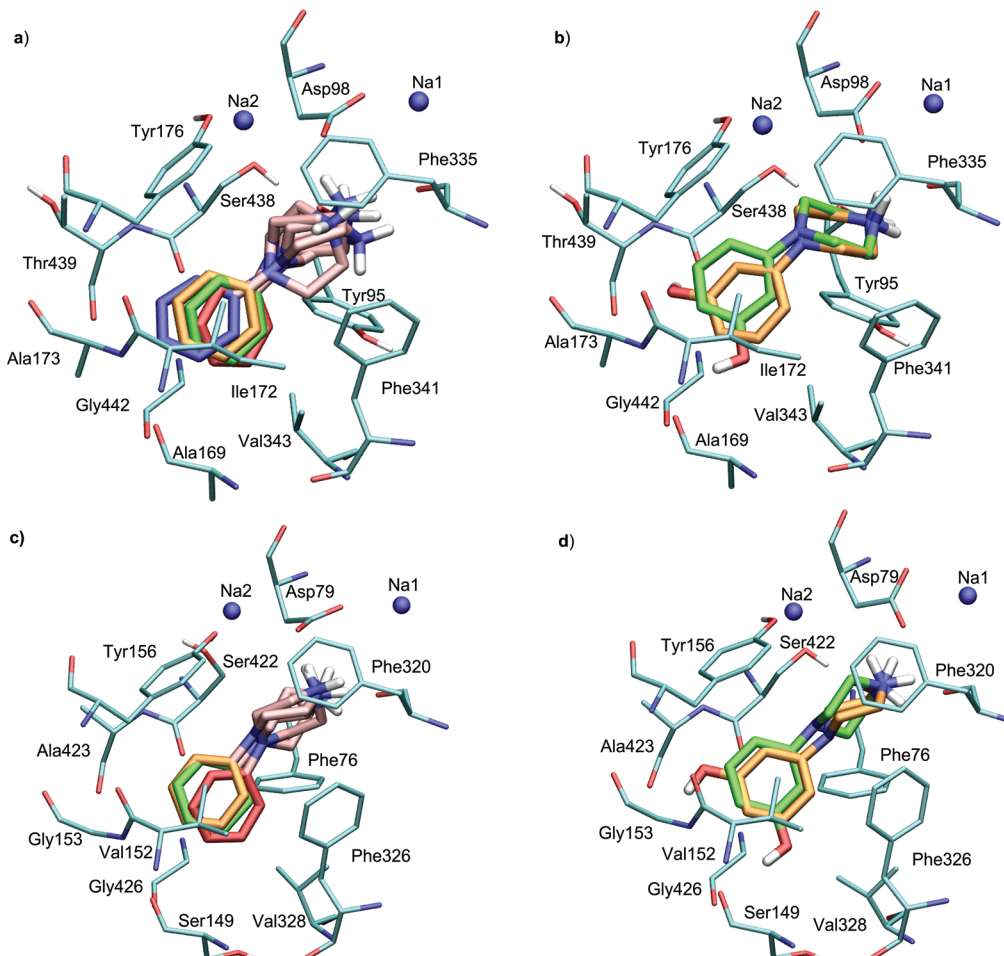


Figure 1. (a) Display of the four subclusters of PP in the binding pocket of hSERT colored by atom type. The protein has carbons atoms shown in cyan, and the piperazine ring is colored pink in all subclusters. Carbon atoms of the phenyl group of PP are colored orange in PP cluster 1, green in PP cluster 2, red in PP cluster 3, and blue in PP cluster 4. (b) Display of the two clusters from the IFD of 3-OH-PP in hSERT, colored by atom type, with carbon atoms of the protein shown in cyan, of 3-OH cluster 1 in orange, and of 3-OH cluster 2 in green. Poses of PP (c) and 3-OH-PP (d) in hDAT are shown using the same color coding as in hSERT in panels a and b.

the distance matrix resulting in the largest separation ratio between clusters (see Figure S1 in the Supporting Information). These are referred to as subclusters PP clusters 1–4, displayed in Figure 1a and are used for the analysis of protein–ligand interactions between PP and hSERT.

The poses of PP with the highest predicted binding affinity to hSERT are found in PP cluster 4 as judged by the computed

average GlideScore (-10.3 kcal/mol). This cluster has an average IFDScore of -961.7 kcal/mol, which is also the most favorable of the four PP subclusters. However, the favorable GlideScore and IFDScore of PP cluster 4 compared with the other subclusters are partly accomplished by a small conformational strain of the ligand as observed from the relatively higher calculated E-model scores in this cluster compared with the

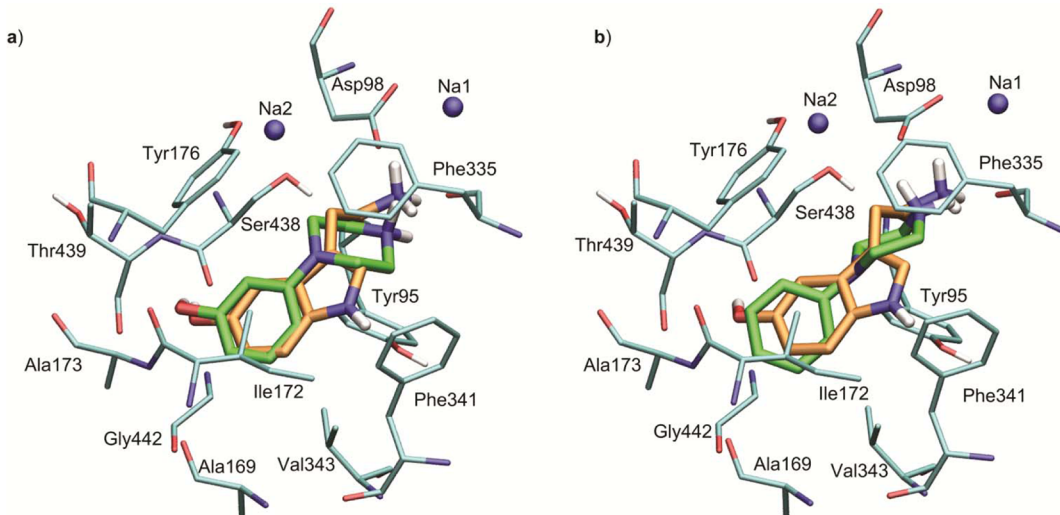


Figure 2. Overlay of typical poses of both 3-OH-PP and PP onto the validated binding mode of 5-HT.¹⁶ In panel a, overlay of a pose from 3-OH cluster 1 (green) and 5-HT (orange). (b) The best overlaying pose of PP (green) and 5-HT (orange).

lowest computed E-model score found in PP cluster 3, see Table 1. By straining PP, it becomes possible for the molecule to sample more local minima on the potential energy surface inside the binding pocket thereby maximizing the interaction with the protein. The energy differences obtained from the IFD docking calculations are however not significantly different for full distinction between the binding modes, but show the same trend. A quantitative method for estimating the strain energy has been developed by Boström et al.²¹ The difference in strain energy is calculated by this method to be only 0.25 kcal/mol between PP cluster 3 and PP cluster 4, which are found to be the geometrically most distant subclusters of PP (see below and Figure 1a, red and blue, respectively). Overall, the strain energy calculated for the four subclusters amounts to less than 3 kcal/mol (0.01 kcal/mol for PP cluster 1, 2.35 kcal/mol for PP cluster 2, 2.36 kcal/mol for PP cluster 3 and 2.51 kcal/mol for PP cluster 4); thus all binding modes represented by subclusters PP clusters 1–4 can be expected to represent the possible biologically active conformations (see the Supporting Information).

All poses exhibit the same overall orientation of the molecule, with the phenyl ring pointing toward Ala173 in one end of the binding pocket and the piperazine moiety pointing toward Asp98 and Phe335 in the other end of the binding pocket. This orientation of the piperazine ring places the charged nitrogen atom in close proximity to these two residues, see Figure 1a. It is apparent from the four subclusters (PP clusters 1–4) in hSERT (Figure 1a) that the nitrogen atom of the piperazine ring is in close proximity to either the backbone carbonyl oxygen of Phe335 or one of the oxygen atoms in the carboxylate group of Asp98. Either way, this can facilitate a hydrogen bond between the charged nitrogen atom and hSERT.²² The existence of a hydrogen bond in the docking poses is judged from the calculated average distances between the charged nitrogen atom in PP and one of the carboxylate oxygen atoms of Asp98, as well as the backbone carbonyl oxygen atom of Phe335, which are both shorter than 3.5 Å.

The 3-OH-PP poses are oriented similar to the PP poses inside the binding pocket of hSERT, inasmuch as the charged nitrogen is facing Asp98 and Phe335 whereas the R₄-position of the phenyl ring points toward Ala173. However, the 3-OH-PP

poses are defined by two distinct clusters with a minimum XCluster separation ratio of 2.25, which is well above the limit of 1.0 for distinguishing two different clusters.^{19,20} Structurally, the two clusters appear to be rotational images of each other with respect to an axis from Asp98 to Ala173 (Figure 1b). The first binding mode (3-OH cluster 1) is positioned with the hydroxyl group pointing in the direction of Ser438 and Thr439, and the other binding mode (3-OH cluster 2) is positioned with the hydroxyl group pointing in the direction of Ala169. This is very similar to what was previously observed for 5-HT binding in hSERT.¹⁶

In our experimentally validated binding mode of 5-HT, the hydroxyl group is located near the backbone of Ser438 and Thr439.¹⁶ By comparing the biochemically validated binding model of 5-HT in hSERT with a pose of 3-OH cluster 1, it becomes evident that the 3-OH-PP could bind in a way very similar to 5-HT, see Figure 2a.

The average GlideScores of 3-OH cluster 1 and 3-OH cluster 2 are −8.9 and −9.4 kcal/mol. By considering the standard deviation, we cannot determine which of the clusters possess the lowest energy. Neither is it possible to distinguish between the clusters by means of the E-model energy (−53.6 and −52.6 kcal/mol) or IFDScore (−962.2 and −963.2 kcal/mol). From the IFD calculations alone, it is thus not possible to conclude which of the two binding modes of 3-OH-PP in hSERT is preferred.

IFD calculations of PP and 3-OH-PP in a homology model of hDAT were also performed (data in Supporting Information). In this calculation, PP is positioned in a very similar manner in hDAT compared with that in hSERT. The charged N₂ atom is pointing toward Asp79 and Phe320 (equivalent to Asp98 and Phe335 in hSERT) and the phenyl moiety is located in the vicinity of Gly153 (equivalent to Ala173 in hSERT) as seen in Figure 1c. The analog 3-OH-PP adopts two distinct binding modes in hDAT like the ones observed in hSERT. In hDAT, the hydroxyl group of 3-OH-PP points toward either Ser149 (equivalent to Ala169 in hSERT) or Ala423 (equivalent to Thr438 in hSERT), as seen in Figure 1d. At this point, it is worth noting that the side-chain functionality of these residues in the two binding pockets is interchanged between hSERT and hDAT, though both residues

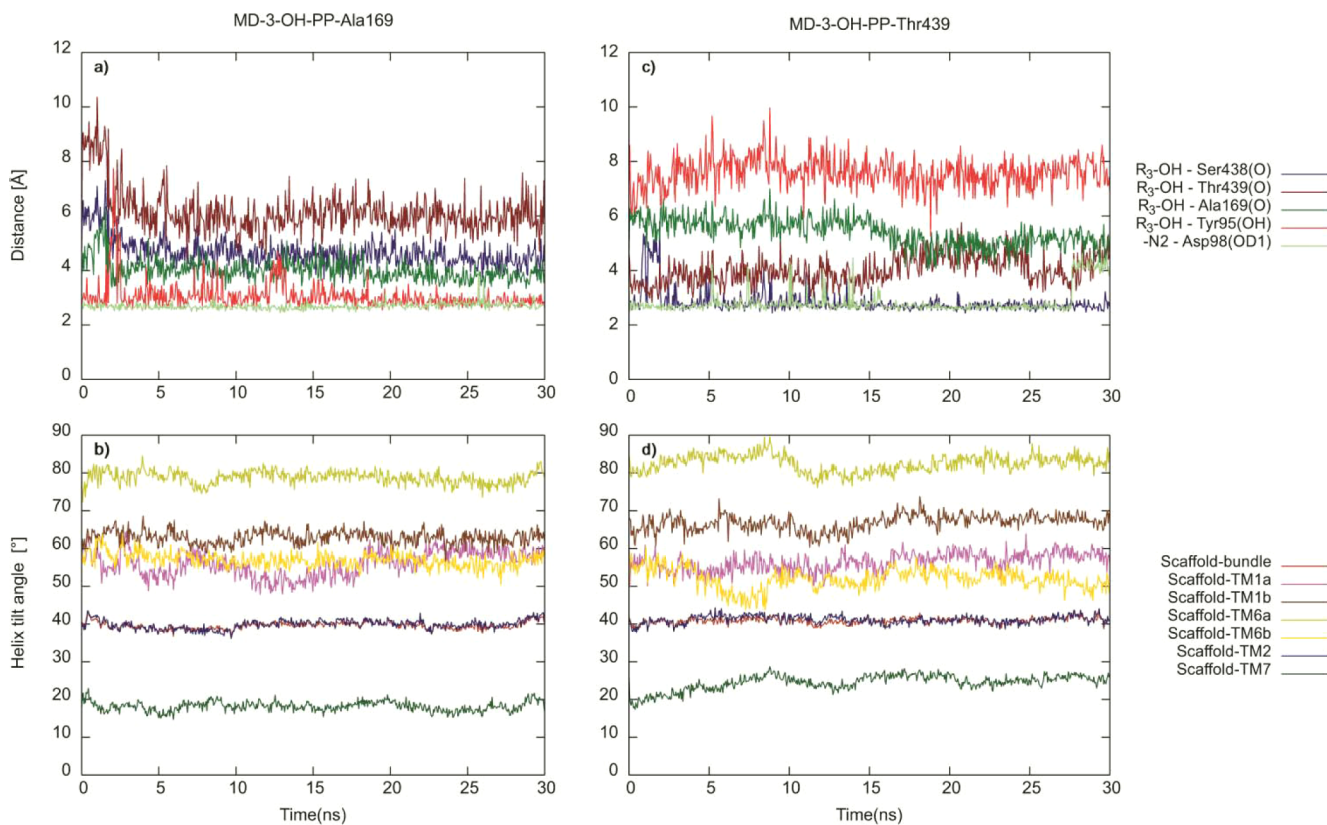


Figure 3. Distances and α -helix tilt angles measured as a function of time for the *MD-3-OH-PP-Ala169* (a, b) and the *MD-3-OH-PP-Thr439* (c, d) simulations.

in question (Ala169 and Thr439 in hSERT and Ser438 and Ala423 in hDAT) have their side chains pointing away from the binding pocket.

MD Simulations. Three 30 ns MD simulations were performed to test the stability of the binding modes identified from IFD. One of the identified binding modes of PP in hSERT and one of each of the two identified possible binding modes obtained from the IFD calculation of 3-OH-PP in hSERT were selected. The first simulation, *MD-PP*, is set up from the lowest GlideScore pose from PP cluster 4. The second simulation uses the pose with the lowest GlideScore from 3-OH cluster 1. In this cluster, the hydroxyl group of 3-OH-PP points toward the hydrophilic pocket formed by Thr439 and Ser438 and is thus referred to as *MD-3OH-PP-Thr439*. The last simulation is setup from the pose with the lowest GlideScore from 3-OH cluster 2 and is referred to as *MD-3OH-PP-Ala169* because the hydroxyl group is located near Ala169.

To measure the stability of the ligands in the binding pockets and of the protein, different metrics were applied. First, the distances from the hydroxyl group of the 3-OH-PP ligand to Tyr95(OH) and the backbone carbonyl oxygen atoms of Ala169, Ser438, and Thr439 were studied. Also the distance from the charged nitrogen atom, N2, in the ligand to the two carboxylate oxygen atoms in Asp98 were measured. These distances indicate the overall stability of the ligand–protein interactions. The tilt angles between a set of protein helices, known as the scaffold, TM3–TM5 and TM8–TM10,²³ and the bundle helices, TM1–2 and TM6–7, are used as the second metric for assessing the conformational stability of hSERT.²⁴

In the *MD-3-OH-PP-Ala169* simulation, the hydroxyl group moves during the initial minimization from a hydrogen bond

interaction with the backbone carbonyl of Ala169 (dark green line in Figure 3a) to a hydrogen bond interaction with the hydroxyl group of Tyr95 (red line). The hydroxyl group of 3-OH-PP forms a transient hydrogen bond with the backbone carbonyl of Gly442 (not shown) after approximately 2 ns and after 12 ns. The interaction between N2 and Asp98 is stable throughout the simulation (light green line). The angle between the scaffold and the bundle of hSERT and between the scaffold and TM2 is observed to remain constant (red and green lines in Figure 3b). Some fluctuations are observed between the scaffold and TM1a, TM1b, TM6a, and TM6b. These two helices contain an unwound part in the center of the helices. These helices are found not to move substantially by visual inspection, and we can conclude that the observed small changes in the tilt angles are caused by the unwound central part of the helices lining the PP binding site.

The hydroxyl group from 3-OH-PP forms a stable hydrogen bond with the backbone carbonyl in Ser438 (blue line in Figure 3c) throughout most of the *MD-3-OH-PP-Thr439* simulation (Figure 3c,d). There are short periods of time during the trajectory where this interaction is temporarily lost, but it quickly reforms. During these short periods, the hydroxyl group of the ligand does not find any other hydrogen bonding partner. The interaction between the N2 nitrogen atom and Asp98 (Figure 3c, light green line) is also stable throughout the simulation. The observed loss of a hydrogen bond after approximately 27 ns is caused by rotation of the carboxylate group of Asp98, thereby forming a hydrogen bond with the other carboxylate oxygen atom instead. Because the negative charge of Asp98 is delocalized on these two oxygens, this reorientation does not reflect a different coordination of the N2

Table 2. Mean K_i Values (μM) Measured for Inhibition of ^3H -5-HT Uptake by HEK-293-MSR Cells Transiently Transfected with Different hSERT Mutants^a

	hSERT	I172T	A173S	A173M	T439A	T439S	V343A	V343L	V343S
PP	6.8	1.48	1.16	0.73	3.8	5.3	10.8	4.0	2.1
2-Me-PP	3.0	1.25	0.50	1.06	4.0	4.3	5.0	0.85	0.83
2-Et-PP	3.9	3.0	3.0	1.16	3.5	6.0	7.1	1.15	1.61
2-SMe-PP	4.8	9.4	1.67	1.13	3.0	6.1	7.1	0.99	1.20
2-OEt-PP	97	250	62	2.8	18.8	82	80	22	13.6
2-CN-PP	118	390	65	16.9	45	50	103	38	26
2-CF ₃ -PP	12.3	17.9	5.3	3.6	8.9	16.6	25	3.6	2.7
2-nitro-PP	20	10.3	6.7	13.0	13.1	19.0	46	7.9	14.3
3-Me-PP	0.93	0.78	0.45	0.20	0.45	1.57	1.69	0.71	0.40
3-OMe-PP	3.0	10.3	1.23	0.22	1.79	3.6	4.5	1.87	1.46
3-OH-PP	7.4	3.1	2.9	6.6	11.9	15.2	12.1	6.3	2.5
4-Me-PP	1.94	1.66	0.65	0.25	1.57	1.23	1.95	0.76	0.77
4-Ac-PP	0.093	0.27	0.072	0.27	0.045	0.079	0.28	0.32	0.154
4-CN-PP	0.30	0.87	0.134	0.103	0.095	0.21	0.63	0.97	0.112
4-OH-PP	6.7	25	4.7	1.79	3.6	5.4	14.8	49	9.4
4-nitro-PP	0.123	0.166	0.041	0.085	0.028	0.038	0.179	0.20	0.071
3,3'-diMeO-PP	14.6	250	6.8	0.75	4.3	13.8	10.4	14.4	
3,3'-Me ₂ OH-PP	9.4	4.1		1.19		8.9			
3,3'-OMe,OH-PP	34	21		7.3		33			
3,3'-OH,OH-PP	9.8	1.85		21		17.1			

^a95% confidence intervals can be found in the Supporting Information.

nitrogen atom. From the analysis of the hydrogen bonding distances and visual inspection, it can be concluded that the ligand remains inside the binding pocket in a stable orientation resembling 3-OH cluster 1. In the *MD-3-OH-PP-Thr439* simulation, the helix tilt angles (plotted as a function of time in Figure 3d) show similar minor fluctuations in their unwound central parts, and we conclude that the protein remains stable during the simulation.

Since PP lacks the hydroxyl functionality, it cannot be expected to be anchored as well in the binding pocket as 3-OH-PP. Indeed, more fluctuations are observed in the *MD-PP* simulation. However, PP remains bound in the binding pocket, forming interactions with the carboxylate group of Asp98 as well as the Phe335 backbone carbonyl group via the charged N2 atom of PP (see Supporting Information). The dihedral angle between the piperazine and the phenyl rings fluctuates more in PP than in 3-OH-PP. Rotations of 180° are observed 21 times during the 30 ns for PP (see Supporting Information). The relative rotation of the phenyl and piperazine rings is not observed at all in the *MD-3-OH-PP-Ala169* simulation and only three times in the *MD-3-OH-PP-Thr439* simulation (see Supporting Information). Furthermore, the piperazine ring of PP is seen to alternate between the chair and the inverted chair conformation 22 times during the *MD-PP* simulation. In contrast, these changes in the conformation of the piperazine ring are only observed twice in the *MD-3-OH-PP-Ala169* simulation (at around 2 ns) and six times in the *MD-3-OH-PP-Thr439* simulation. This indicates that 3-OH-PP contains less conformational flexibility when bound to hSERT compared with PP. In conclusion, the MD simulations reveal that on the 30 ns time scale, the ligand binding modes observed from IFD are stable and that the ligands are bound in the central binding pocket of hSERT, which hereby provide models that can be tested experimentally.

Biochemical Results. The results of the IFD calculations of PP and 3-OH-PP in hSERT and hDAT suggested a very flexible binding mode for PP in the primary binding pocket whereas the

orientational and conformational space for 3-OH-PP was more defined. The aim of our biochemical experiments is to validate the predicted binding modes of PP and 3-OH-PP inside the primary binding site of hSERT and hDAT by using different substituents on the phenyl ring of PP. Additionally, we aim at providing more detailed information on how different types of substitutions on PP may dictate specific binding conformations of the PP skeleton.

PP in hSERT. A broad repertoire of different analogs, see Table 2, was tested for their inhibitory potencies in a cell-based S-HT radiotracer uptake assay assessing both wt hSERT and a collection of eight rationally chosen hSERT mutants in order to explore the predicted binding mode of PP. The mutants were chosen based on the position of the amino acids in the binding pocket in order to cover the bulk of the binding pocket surrounding the aromatic part of PP. At each position, mutations were chosen preferably in pairs, which were equal in size but different in their polarity, one hydrophilic and one hydrophobic. The eight hSERT mutants examined were Ile172Thr, Ala173Ser, Ala173Met, Thr439Ala, Thr439Ser, Val343Ala, Val343Leu, and Val343Ser.

Exploration of the Environment around R₂ of PP. The R₂ position of PP was examined using the compounds 2-Me-PP, 2-nitro-PP, 2-Et-PP, 2-SMe-PP, 2-CN-PP, 2-OEt-PP, and 2-CF₃-PP, which provide substituents with varying length and polarity, see Chart 1. The inhibitory potencies of R₂-substituted PP analogs suggest that the space around the R₂-position of PP can accommodate a methyl or an ethyl substituent with measured K_i values of 3.0 μM ($p = 0.0019$ compared with PP) and 3.9 μM ($p = 0.0162$ compared with PP), respectively, showing a 2-fold better binding than PP (K_i of 6.8 μM) see Table 2. The environment also appears to be hydrophobic because introduction of either a trifluoromethyl or a nitro group decreases the affinity to 12.3 μM ($p = 0.0265$) and 20 μM ($p < 0.0001$), respectively. These two substituents are approximately equal in size to methyl and ethyl but more polar than the aliphatic groups. Increasing the length of the R₂-substituent

strongly decreases the binding potential compared with PP as seen with 2-OEt-PP and 2-CN-PP with K_i values of 97 μM ($p < 0.0001$) and 118 μM ($p < 0.0001$), respectively. R₂-substituted PP analogs were tested against the eight mutants included in Table 2 to locate protein–ligand contact points near the R₂-position of PP. The relative inhibitory potencies of 2-OEt-PP and 2-CN-PP decrease 15-fold in the Ile172Thr mutant compared with wt hSERT ($p = 0.23$ and $p = 0.0453$, respectively). Since threonine is smaller than isoleucine the loss of affinity cannot be ascribed to a simple steric repulsion; rather it seems to be an effect of changing the hydrophobic nature of isoleucine to the more hydrophilic threonine.

From our previous study,¹⁶ it is known that mutation of Ala173 and Thr439 can affect the environment in a hydrophilic pocket housing the hydroxyl group of the cognate substrate, 5-HT. The K_i values of 2-OEt-PP in the Ala173Ser, Ala173Met, Thr439Ser, and Thr439Ala mutants suggest that the hydrophobic moiety of the OEt-group can reach into this pocket. When the nature of the pocket is changed to a more hydrophilic environment with the Ala173Ser mutation, a clear tendency to decreased inhibitory potency of 2-OEt-PP relative to PP is found ($K_{i,2\text{-OEt-PP}}/K_{i,\text{PP}}$ changes from 14.2 in wt to 53.4 in Ala173Ser, $p = 0.0865$), whereas the opposite applies for the mutations Ala173Met and Thr439Ala partially reversing the hydrophilic surroundings to more hydrophobic ones.

Exploration of the Environment around Position R₃ of PP. The environment surrounding the R₃-substituent was examined with compounds 3-OMe-PP, 3-Me-PP, and 3-OH-PP. Since PP is completely symmetrical, a substitution at the R₃-position of the phenyl moiety can orient toward two different parts of the binding pocket, if allowed by the protein. From the IFDs of PP in both hSERT and hDAT, it is observed that the R₃- and R_{3'}-positions are pointing toward the hydrophilic pocket, lined by Ala173 and Thr439, and toward the hydrophobic Ile172 residue, respectively. If the unsubstituted aromatic part of the PP skeleton in itself is relatively flexible in the binding site as the IFD and MD simulations suggest, it should be expected that a hydrophobic substituent at the R₃-position would orientate toward Ile172 and a hydrophilic substituent toward the hydrophilic pocket. In the Ala173Met mutant both binding pockets become hydrophobic, which is consistent with an observed relative 8-fold loss in affinity for placing a hydrophilic hydroxyl group at the R₃-position of the PP skeleton (3-OH-PP, $p = 0.173$). In the Ile172Thr construct both contact points become hydrophilic, which is consistent with a 10-fold relative loss of affinity when a hydrophobic substituent is introduced at the R₃-position (3-OMe-PP, $p = 0.0407$) (Figure 4a,b). If one of the R₃-substituents is pointing toward the hydrophilic pocket and the other, for disubstituted analogs, is pointing into the pocket with Ile172, an even larger loss in affinity in the Ile172Thr mutant would be expected for 3,3'-diOMe-PP. Indeed, we observe an 80-fold relative decrease in affinity for 3,3'-diOMe-PP in Ile172Thr ($p = 0.0026$) (Figure 4a,c). This extensive loss of inhibitory potency seems not to be caused by steric conflict since 3,3'-diOMe-PP in all other mutants has inhibitory potencies comparable to wt hSERT. Similarly, we would expect a larger decrease in affinity for the compound 3,3'-diOH-PP in the Ala173Met mutant in which both the expected pockets for the 3 and the 3' positions are hydrophobic in nature. Completely in line with this expectation, we see a 20-fold reduction in relative affinity for this double-hydrophobic substituted PP analog.

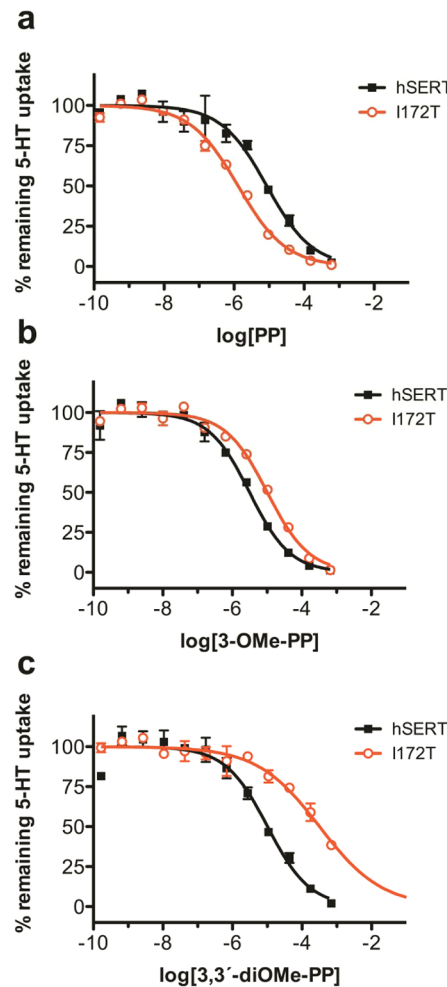


Figure 4. IC₅₀ curves of inhibition of radiotracer 5-HT uptake in HEK-293-MSR cells transiently transfected with wt hSERT or Ile172Thr with PP (a), 3-OMe-PP (b), 3,3'-diOMe-PP (c).

Exploration of the Environment around R₄-Position of PP. The R₄-position of PP was examined using the compounds 4-Ac-PP, 4-nitro-PP, 4-OH-PP, 4-Me-PP, and 4-CN-PP. Introducing a substituent at the R₄-position of PP has in all constructs, except for 4-OH-PP, a positive effect on the inhibitory potency with a maximum effect reaching 70-fold decreased K_i for 4-Ac-PP compared with wt hSERT, K_i values of 0.093 and 6.8 μM , respectively ($p < 0.0001$).

In the four subclusters identified from IFD of PP in hSERT, the R₄-position is pointing toward Ala173 in PP cluster 1 and moves gradually toward the bottom of the binding pocket closer to Val343 in PP cluster 4. None of the poses from the IFD of PP appear to leave much space between the R₄-position of PP and Ala173. Therefore, we hypothesize that most substituents at the R₄-position will be placed with the group pointing toward Val343 where more space is available. In line with this, all R₄-substituted PPs are equipotent or superior to PP with the small hydrophilic hydroxy-group affecting potency the least.

Selectivity between Monoamine Transporters. To gain insight into the molecular determinants of PP analog selectivity for the different monoamine transporters, we tested the affinity for eight PP analogs in inhibition of uptake in HEK-293-MSR cells transiently transfected with hSERT, hDAT, or hNET cDNA (Table 3). Furthermore, because an important

Table 3. K_i Values for Inhibition of Radiotracer Uptake in HEK-293-MSR cells transiently Transfected with hSERT, hDAT, or hNET cDNA^a

compound	K_i values (μM) for inhibition of uptake			hDAT/hSERT	hNET/hSERT	hDAT/hNET
	hSERT	hDAT	hNET			
PP	6.8 [4.6–9.9]	6.9 [1.47–33]	0.58 [0.19–1.75]	1.01	0.084	11.9
2-Me-PP	3.0 [2.3–3.9]	2.8 [1.28–6.1]	0.06 [0.004–0.92]	0.93	0.02	47
3-Me-PP	0.93 [0.59–1.46]	31 [16.8–56]	2.8 [0.35–23]	33	3.0	11.1
3-OMe-PP	3.0 [2.5–3.6]	50 [22–112]	10.7 [0.31–370]	16.7	3.6	4.7
3-OH-PP	7.4 [5.0–11.0]	3.5 [1.69–7.0]	0.68 [0.27–1.74]	0.47	0.092	5.1
4-Me-PP	1.94 [1.12–3.4]	19.2 [13.5–27.4]	2.1 [0.39–11.4]	9.9	1.08	9.1
4-CN-PP	0.30 [0.2–0.46]	149 [96–230]	13.6 [5.1–36]	500	45	11.0
4-OH-PP	6.7 [4.8–9.2]	4.4 [1.73–11.4]	0.60 [0.26–1.4]	0.66	0.090	7.3

^a95% confidence intervals are shown in brackets, $n \geq 3$.

Table 4. EC₅₀ Values \pm SEM from Release of Accumulated Neurotransmitter in Synaptosomes Prepared from Rat Brain

PP analog	release EC ₅₀ (nM)			DAT/SERT	NET/SERT	DAT/NET
	SERT	DAT	NET			
PP	880 \pm 114	2,530 \pm 210	186 \pm 18	2.9	0.21	13.6
2-Me-PP	175 \pm 13	540 \pm 43	39 \pm 5	3.1	0.22	13.8
2-CF ₃ -PP	570 \pm 61	11200 \pm 560	350 \pm 64	19.6	0.61	32
2-SMe-PP	270 \pm 14	>10000	>10000	>37	>37	
2-Et-PP	290 \pm 24	>10000	830 \pm 113	>35	2.8	>12
2-chloro-PP	310 \pm 40	>3000	26 \pm 2.5	>10	0.087	>118
2-bromo-PP	132 \pm 16	250	33 \pm 2.8	1.89	0.25	7.6
2-nitro-PP	1870 \pm 230	>10000	770 \pm 77	>5	0.41	>13
3-fluoro-PP	115 \pm 15	2400 \pm 220	340 \pm 77	21	3.0	7.1
3-Me-PP	110 \pm 12	>20000	>20000	>182	>182	
3-OMe-PP	650 \pm 32	>10000	>10000	>15	>15	
3-OH-PP	230 \pm 15	2500 \pm 156	174 \pm 12	10.8	0.75	14.3
4-fluoro-PP	230 \pm 29	>10000	3200 \pm 480	>44	13.9	>3
4-Me-PP	220 \pm 20	>20000	>10000	>91	>46	
4-OMe-PP	nd	6300 \pm 390	440 \pm 39			14.3
4-Ac-PP	50 \pm 5.1	3000 \pm 330	150 \pm 16	60	3.0	20
4-CN-PP	36 \pm 1.2	>10000	6300 \pm 700	>280	176	>0.16
4-Phenyl-PP	>10000	5200 \pm 510	1520 \pm 350	<0.52	<0.152	3.4
4-OH-PP	>10000	850 \pm 55	230 \pm 42	<0.085	<0.023	3.7
4-nitro-PP	19 \pm 4.6	>10000	>10000	>530	>530	
2,3-dichloro-PP	10 \pm 0.6	108 \pm 9	36 \pm 2.9	10.8	3.6	3.0
2,3-diMe-PP	24 \pm 6.4	1320 \pm 740	13.7 \pm 2.1	56	0.57	96
2,4-difluoro-PP	470 \pm 39	>10000	2300 \pm 230	>21	4.9	>4.3
3,4-difluoro-PP	76 \pm 9.1	>10000	9200 \pm 970	>131	120	>1.09

characteristic of the PP compounds is their ability to induce release of accumulated neurotransmitter, we also determined EC₅₀ values for a broader repertoire of PP analogs in a release experiment performed on synaptosomes prepared from rat brain (Table 4).

Because understanding and controlling the selectivity between the monoamine transporters is expected to be vital to the development of efficient cocaine addiction pharmacotherapies,^{10–13,25,26} we aimed at determining important attributes of PP that might dictate the nature of their individual preferences. The K_i values from inhibition of uptake for the eight employed PP analogs in hSERT, hDAT, and hNET are listed in Table 3, and the EC₅₀ values for release are listed in Table 4.

The results from inhibition of uptake show that hNET has the highest affinity of the three transporters for the unsubstituted PP with affinity 12-fold higher than both hSERT ($p < 0.0001$) and hDAT ($p = 0.011$). The selectivity, however, is clearly dependent on the presence and position of a

substituent. 3-Me-PP has more than 30-fold higher affinity ($p < 0.0001$) for hSERT than hDAT with K_i values of 0.93 and 31 μM respectively, whereas a hydroxyl group in the 3-position, 3-OH-PP, only has very modest effect on the selectivity compared with PP. Also, the type of substituent on the 4-position has a large impact on selectivity because 4-OH-PP has essentially the same selectivity profile as PP whereas 4-CN-PP favors hSERT 300-fold over hDAT ($p < 0.0001$) and 40-fold ($p < 0.0001$) over hNET.

In an attempt to address the observed differential binding that some of these ligands demonstrate between hSERT and hDAT, the binding pockets were analyzed for changes in amino acid composition between the two closely related transporters. Within 4 Å of the ligand bound in hDAT and hSERT, there are eight diverging residues; Tyr95 (Phe76 in hDAT), Ala169 (Ser149 in hDAT), Ile172 (Val152 in hDAT), Ala173 (Gly153 in hDAT), Tyr175 (Phe155 in hDAT), Thr439 (Ala423 in hDAT), Leu443 (Met427 in hDAT), and Thr497 (Ala480 in hDAT). We mutated these positions in hSERT to the

corresponding residues in hDAT and *vice versa* for hDAT. Moreover, mutants were combined in each of the two wt contexts to create the Y95F_I172V, Y95F_L443M, and Y95F_I172V_L443M constructs in hSERT, and the reverse F76Y_V152I, F76Y_M427L, and F76Y_V152I_M427L constructs in hDAT. The resulting 22 mutants were tested against PP, and seven PP analogs were selected to reveal potential key amino acid residues and positions of the PP phenyl ring that cooperatively provide the discrimination between the two transporters (K_i values can be found in Supporting Information, Tables S7 and S8). It was, however, not possible to pinpoint positions inside the binding pocket that would reverse the selectivity by changing the nature of one hDAT residue into the corresponding in hSERT or *vice versa*. The selectivity may be a composite of several minor contributions from residues within the binding site or even from indirect contributions from residues outside the binding site.

The selectivity data from the release experiment (Table 4) are in concert with the data from inhibition of uptake. It is noteworthy that very small differences have drastic effects on selectivity as seen from the uptake experiment. When 2-Me-PP and 2-SMe-PP are compared, the potency of the compounds for effecting release changes from being modestly hNET selective with reasonable affinity for all three transporters to becoming highly hSERT selective with at least 30-fold higher affinity for hSERT over both hDAT and hNET. As is also seen in the uptake experiments, the substituent on the 4-position of PP has enormous influence on the selectivity. 4-OH-PP favors hNET more than 10-fold over hSERT and hDAT, whereas 4-nitro-PP favors hSERT at least 500 times over both hDAT and hNET. These correlations between the potency in uptake inhibition and efflux suggest that the PP compounds effect inhibition and efflux via the same site and the same binding mode. This is fully consistent with PP compounds competing with 5-HT for the central substrate site and eliciting neurotransmitter efflux by being substrates themselves and exchanging for intracellular neurotransmitter as described in the alternating access model.

To some of the tested compounds, it applies that the difference in affinity between transporters is much larger in the release experiment than seen for inhibition of uptake. Species differences in pharmacological profile between rat and human monoamine transporters may account for some of this difference. The difference may however, also be ascribed to the fact that release not only requires binding but also transport of the releaser, which thereby causes the protein to adopt an inward facing conformation from which it can carry accumulated neurotransmitter out across the cell membrane.

CONCLUSION

The data from induced fit docking and molecular dynamics simulations of phenylpiperazine (PP) in the human serotonin transporter (hSERT) and the human dopamine transporter (hDAT) together with structure–activity relationship data from hSERT mutants strongly suggest that PP binds inside the primary substrate binding pocket of the monoamine transporters. The data also show that binding of PP is not restricted to a single conformational state during binding. Rather it is suggested by the data that the binding is promiscuous such that the ligand has multiple energy minima in which a strong interaction between the positively charged amine and the negatively charged Asp98 in hSERT or the hDAT/hNET equivalent is maintained whereas the unsubstituted phenyl

moiety is allowed to rotate almost freely between at least four different binding states. In contrast, substituted PP analogs have less flexibility in the binding pocket as seen for 3-OH-PP in the MD simulations and supported by the structure–activity relationship data.

The combined data from inhibition of uptake and induction of release in the monoamine transporters together with induced fit docking and molecular dynamics simulations of PP compounds bound to homology models of hSERT and hDAT explicitly suggest that the PP compounds indeed bind to all three transporters in the primary binding site. This is in full agreement with the simplest way of explaining how this type of compound elicits reverse translocation of neurotransmitter through the monoamine transporters, namely, by being substrates themselves and as such competing with the cognate substrate for the substrate binding site and after release to the intracellular space allowing binding and translocation of neurotransmitter in the reverse direction.

We have provided a detailed pharmacological characterization of how a large repertoire of substituents can change the selectivity of PP analogs between the transporters in both inhibition of uptake and release of accumulated neurotransmitter. In line with previous studies, we could eliminate the release effect on hNET and at the same time keep the release effect on hSERT.²⁷ However, it was not possible to eliminate NET release activity without simultaneously eliminating DAT release activity. The complexity of hSERT/hDAT/hNET selectivity is stressed by the observations that we were unable to pinpoint residues within the binding site that accounted for the changes in selectivity that we found for some of the PP compounds. These results suggest that no single residue accounts for the differences in monoamine selectivity of PP analogs but that it may be a composite of numerous small contributions and promiscuous binding.

We identified PP analogs that were highly selective for hSERT over hDAT and hNET (4-CN-PP), for hNET over hDAT and hSERT (2-chloro-PP), for hDAT and hNET over hSERT (4-OH-PP), and finally for hNET and hSERT over DAT (4-Ac-PP). These findings clearly show how fine-tuning of a simple scaffold, such as the PP skeleton, with small substituents can deliver high selectivity between closely related proteins exemplified in this study by the monoamine transporters.

METHODS

Homology Model and Protein Modeling. The homology model of hSERT used in this study is based on the published alignment²⁸ of hSERT, which uses the structure of the bacterial leucine transporter (LeuT)²⁹ as template. Further details of the homology modeling is found in the study of 5-HT binding to hSERT.¹⁶ The model includes the two sodium ions close to the binding site but does not include a chloride ion, which was proposed to be placed in the vicinity of the binding site of chloride-dependent transporters.^{30,31} The presence of this ion was shown to neither influence the predicted binding of the native ligand of hSERT in docking calculations nor affect the placement of PP in test computations. The protein was initially prepared using the Protein Preparation facility in the Schrödinger suite of software and has been previously described for hSERT.¹⁶

The homology model of hDAT was likewise modeled with the LeuT as a template and is also based on a sequence alignment by Weinstein and co-workers. The model contains two sodium ions as found in the LeuT crystal structure, and a chloride ion was included at the suggested chloride ion binding site.

Ligand Modeling. All ligand modeling calculations are carried out using the Schrödinger 7.5 suite.³² PP was built in Maestro and energy minimized by the steepest descent method for 50 iterations followed by complete minimization by the Polak and Ribiere conjugate gradient method³³ until convergence after 240 iterations. The minimizations were done using the MMFFs force field³⁴ because it has parameters for planar sp² nitrogen atoms, which is expected for the N1 nitrogen atom of PP. The N2 atom of PP is modeled with a single positive charge, see Chart 1.

The optimized structure was then subjected to a Metropolis Monte Carlo simulation using the MCMM method implemented in MacroModel version 9.1³² sampling 25 000 iterations. This resulted in 14 unique conformations. Of these, the one with the lowest energies were selected for each of the four possible conformations of a monosubstituted piperazine ring: twist boat (T) or chair (C) of the six-membered ring and the two positions, axial (A) or equatorial (E), of the phenyl substituent at N1 (see Chart 1). The four conformations of the piperazine ring in PP and 3-OH-PP are referred to as CA (chair–axial), CE (chair–equatorial), TA (twist boat–axial), and TE (twist boat–equatorial) and were used as input structures of the ligand in the docking calculation. The input structures for the docking study of 3-OH-PP were built by adding a hydroxyl group at the R₃-position of the phenyl group on each of the four PP input conformations.

Induced Fit Docking. To accommodate the ligand in the substrate binding pocket the IFD protocol was used.^{35,36} This solution employs both Glide version 4.0 and Prime version 1.5 methodology from the Schrödinger 2006 suite of programs. This technique allows parts of the protein to be flexible during the docking calculations. IFD involves an initial soft docking using Glide and the standard precision (SP) scoring function.³⁷ To incorporate protein flexibility, a second step follows, where the protein is refined in Prime within 5 Å of the substrate. Finally the ligand is redocked in Glide using the optimized structure of the binding pocket and the extra precision (XP) scoring function implemented in Glide.³⁸ The GlideScore is an empirical scoring function that accounts for the interaction energy between the ligand and the protein and approximates the ligand binding free energy.³⁷ The Prime energy provides an estimate of the protein energy after the second step in the IFD protocol. The IFDScore is a combination of the GlideScore and the Prime energy, and the developers suggest that docking poses are different when the IFDScore of two poses differs by more than 0.2 kcal/mol.³⁶ The E-model score is a combination of the GlideScore, the nonbonded interactions, and the internal strain of the ligand and is used in Glide for pose selection when the GlideSP-scoring function is used.

The IFD calculations were performed with the default settings, and the binding pocket was defined from Asp98 and Ile172 in hSERT and Asp79 and Val152 in hDAT, indicating that these residues determine the center of the docking box. Sixteen IFD calculations were carried out, one for each of the four identified low-energy conformations of the two substrates, PP and 3-OH-PP, in the two proteins.

Analysis of Poses. The resulting poses from the IFD calculations were subjected to a cluster analysis using the XCluster^{19,20} facility available in the Schrödinger 2006 program suite. Details of the XCluster analysis are supplied in the Supporting Information.

Conformational Energy of Bound Ligand. Boström et al.²¹ have proposed that biologically active conformations should be within 3 kcal/mol of the global energy conformation as calculated with an implicit solvation model (GB/SA).³⁹ This methodology was adapted: First, a conformational search using MacroModel version 9.6⁴⁰ was performed of PP using the Optimized Potentials for Liquid Simulations All Atom, version 2005, force field (OPLS_2005),^{41,42} resulting in the identification of nine minimum energy conformations. Then, a representative pose for each of the four subclusters from the IFD of PP in hSERT were selected, and rmsd calculations were performed between the pose and each of the nine minimum energy structures. The strain energy in the protein bound conformation of the ligand is found as the energy difference between the energy of this conformation and the global minimum energy in implicit solvent.²¹

Molecular Dynamics Simulations. The simulations were set up in Desmond by using the workflows provided in Maestro. The MD

simulations were run using the Desmond program version 2.2.^{43–45} The procedure for the three simulations was the same. The best scoring poses with respect to GlideScore from the IFD of PP and 3-OH-PP were used as input structures. A membrane was added using the Desmond system builder tool accessible from the applications menu in Maestro. The membrane chosen was 1-palmitoyl-2-oleoyl-3-sn-phosphatidylcholine (POPC) as a single constituent. The box was defined to be 10 Å larger than the protein in the x-, y- and z-directions, and the solvent used was TIP3P.⁴⁶ The OPLS_2005^{41,42} force field was used, and the SHAKE algorithm⁴⁷ was applied. Accordingly, the time step was set to 2 fs. The simulations were performed at 310 K with the temperature controlled by a Berendsen-type thermostat,⁴⁸ and a time constant of 1 ps. The pressure was kept at 1 bar using a Berendsen-type barostat with a 2 ps time constant and a compressibility of 4.5×10^{-5} bar⁻¹ semi-isotropic pressure regulation. Short range electrostatic interactions were calculated with a cutoff of 9 Å, and the long-range interactions were calculated with PME.^{49,50} All simulations were carried out with periodic boundary conditions.

Helix Tilt Angles. The hSERT consists of 12 transmembrane helices TM1 to TM12. From these, it is possible to define a scaffold consisting of TM3, TM4, TM5, TM8, TM9, and TM10 and a bundle of helices proposed to be move during transport, TM1, TM2, TM6, and TM7.²³ The helix tilt angles were calculated between the vectors describing the scaffold and the different helices in the bundle.

The N- and C-terminus end points of the helices describing the vector of the scaffold have been defined as the center of mass of the four residues in each end of the helices TM3–5 and TM8–10. The vector used to describe the bundle (TM1a, TM1b, TM2, TM6a, TM6b, and TM7) is found in the same way.

Ligand Synthesis. [³H]-5-HT and [³H]-DA were purchased from PerkinElmer Life Science. All PPs were purchased commercially except for 3,3'-Me-OH-PP, 3,3'-OMe-OH-PP, and 3,3'-diOH-PP. These three compounds were synthesized by condensation of N-benzyl-protected phenylpiperazine with the appropriately substituted resorcinol (5-methyl-, 5-methoxy-, and 5-hydroxyresorcinol, respectively) in refluxing toluene.

Mutagenesis. Site-specific mutations of hSERT were introduced using Phusion High-Fidelity DNA polymerase (Finnzymes) and mismatched primer pairs. XL-10 Gold *Escherichia coli* (Stratagene) were transformed and used for DNA production. DNA was purified using the GenElute (SigmaAldrich) miniprep kit or the PureYield (Promega) midiprep kit according to the manufacturer instructions. All mutants were sequenced across the full reading frame to ensure that no unwanted secondary mutations had been introduced.

Cell Culture and Expression in HEK-293-MSR Cells. The human embryonic kidney cell line HEK-293-MSR (Invitrogen) was grown in monolayer in Dulbecco's modified Eagle's medium (DMEM) supplemented with 10% fetal bovine serum, 600 µg/L streptomycin, 100 units/L penicillin and 0.1 mM nonessential amino acids. Cells were cultured at 37 °C with constant CO₂ concentration at 5% and humidity at 95%. For transfections, 0.2 µg of plasmid and 0.4 µg of Lipofectamine 2000 reagent (Invitrogen) were used per square centimeter of plating area. Plasmid and Lipofectamine 2000 reagent were mixed with DMEM according to the manufacturers' recommendations. HEK-293-MSR cells were trypsinized, suspended in growth media, and added to the plasmid/Lipofectamine complex. Transfected cells were seeded in white 96-well growth plates (Corning) at 60–80% confluence.

5-HT Uptake Assay. Uptake assays were performed 40–50 h after transfection. For IC₅₀ determinations, transfected cells were washed with phosphate-buffered saline (PBS; 137 mM NaCl, 2.7 mM KCl, 4.3 mM Na₂HPO₄, 1.4 mM KH₂PO₄) supplemented with 0.1 mM CaCl₂ and 1 mM MgCl₂ (PBSCM) at pH 7.4 and immediately preincubated for 25 min at RT with 30 µL of the PP analog using 12 increasingly concentrated solutions of the compound dissolved in PBSCM. The uptake was initiated by adding 30 µL of compound dissolved in PBSCM containing [³H]5-HT to a final 5-HT reaction concentration of 70–100 nM. Incubation proceeded 10 min before aspiration and washing in PBSCM terminated the assay. For $K_m - V_{max}$ determin-

nations, transfected cells were washed with PBSCM buffer and immediately preincubated for 25 min at RT with 30 μ L of either PBSCM to determine total uptake or 200 μ M S-citalopram in PBSCM to determine nonspecific uptake. The assay was initiated by the addition of 30 μ L of [³H]5-HT diluted 15 times with unlabeled 5-HT in increasing concentrations. The assay was terminated after 10 min by aspiration and washing in PBSCM. Cells were lysed in 50 μ L of MicroScint-20 (Packard) and the radiolabeled 5-HT accumulated in the cells was quantitated in a Packard TopCounter NXT microplate scintillation counter.

Animals. Male Sprague–Dawley rats (Charles River, Wilmington, MA) weighing 300–400 g were used as subjects in the release experiment. Rats were housed in standard conditions (lights on from 0700 to 1900 h) with food and water freely available. Animals were maintained in facilities fully accredited by the Association for the Assessment and Accreditation of Laboratory Animal Care (AAALAC), and experiments were performed in accordance with the Institutional Care and Use Committee of the National Institute on Drug Abuse (NIDA), Intramural Research Program (IRP).

Drugs and Reagents. [³H]MPP⁺ (SA = 85 Ci/mmol), [³H]5-HT (SA = 27.5 Ci/mmol), and [³H]DA (SA = 31.8 Ci/mmol) were purchased from PerkinElmer (Shelton, CT). The sources of other reagents are published.^{27,51}

In Vitro Release Methods. Transporter-mediated release assays were carried out as previously described with minor modifications.⁵² Rats were sacrificed by CO₂ asphyxiation. Tissue from caudate (for DAT assay), or from whole brain minus cerebellum and caudate (for SERT and NET assay), was homogenized in ice-cold 10% sucrose containing 1 μ M reserpine. For DAT-mediated release assays [³H]1-methyl-4-phenylpyridinium (³H]MPP⁺) was used as the radiolabeled substrate; 100 nM desipramine and 100 nM citalopram were added to prevent uptake of [³H]MPP⁺ into NE and 5-HT nerves. For SERT-mediated release assays, [³H]5-HT was used as the radiolabeled substrate; 100 nM nomifensine and 50 nM GBR12935 were added to the sucrose solution to prevent uptake of [³H]5-HT into NE and DA nerve terminals. For the NET-mediated release assay, 50 nM GBR12935 and 100 nM citalopram were added to block [³H]MPP⁺ uptake into DA and 5-HT nerves. Synaptosomal preparations were incubated to steady state with 5 nM [³H]MPP⁺ (60 min) or 5 nM [³H]5-HT (60 min) in Krebs-phosphate buffer (pH 7.4), plus 1 μ M reserpine. Subsequently, 850 μ L of synaptosomes preloaded with [³H]ligand were added to polystyrene test tubes that contained 150 μ L of test drug in assay buffer plus 1 mg/mL BSA. After 5 min ([³H]5-HT) or 30 min ([³H]MPP⁺), the release reaction was terminated by dilution with 4 mL of wash buffer followed by rapid vacuum filtration. Nonspecific values were measured by incubations in the presence of either 100 μ M tyramine ([³H]5-HT release assay) or 10 μ M tyramine ([³H]MPP⁺ release assays). The retained tritium was counted by a Topcount liquid scintillation counter (PerkinElmer, Shelton, CT).

Data Analysis and Statistics. For release experiments, dose–response curves were generated using eight concentrations of test drug. In order to describe the method for calculating the release dose–response curves, the following definitions are necessary:

total binding (TB) = cpm in the absence of any drug.

nonspecific binding (NS) = cpm in the presence of tyramine.

maximal release (MR) = TB – NS

specific release (SR) = (cpm in the presence of drug) – NS

% MAX release = 100 – SR/MR × 100.

The data of three experiments, expressed as % MAX release were then fitted to a dose–response curve model: $Y = E_{\text{MAX}}([D]/([D] + EC_{50}))$ for the best fit estimates of the E_{MAX} and EC_{50} using either KaleidaGraph version 3.6.4 or MLAB-PC.⁵³

ASSOCIATED CONTENT

S Supporting Information

Tables of all docking poses, details of theory behind XCluster and the results of the cluster analysis, as well as computations on PP conformations, and 95% confidence intervals of the uptake inhibition assays of wt hSERT and hDAT and all mutant constructs. This material is available free of charge via the Internet at <http://pubs.acs.org>.

AUTHOR INFORMATION

Corresponding Author

*E-mail: birgit@chem.au.dk or steffen.sinning@cpf.au.dk. Fax: +45 7847 1115. Phone: +45 7847 1108.

Author Contributions

K.S. and J.F.K. contributed equally. K.S. and K.A.V. carried out the SAR experiments. J.F.K. did the docking and MD simulations. H.K. did the homology modeling and assisted with docking and MD simulations. B.B. performed the synthesis of PP analogs. K.S., B.S., and S.S. planned the project and wrote the manuscript with assistance from H.K. R.B.R. and J.S.P. contributed the synaptosomal in vitro release data, and R.B.R. contributed to writing the manuscript.

Notes

The authors declare no competing financial interest.

ACKNOWLEDGMENTS

The research was supported by grants from the Lundbeck, Carlsberg, and Novo Nordisk Foundations, the Danish Strategic Research Council, the Danish National Research Foundation, and the National Institute of Drug Abuse (USA, Grant DA12790). Computations were possible through allocations of time at the Centre for Scientific Computing, Aarhus. We thank Aarhus Graduate School of Science (AGSoS) and iNANOSchool for financial support. Portions of this work were supported by the Intramural Research Program, National Institute on Drug Abuse, NIH, DHHS, Baltimore, MD.

ABBREVIATIONS

hSERT, human serotonin transporter; hDAT, human dopamine transporter; 5-HT, 5-hydroxytryptamine; DA, dopamine; PP, 1-phenyl-piperazine; 3-OH-PP, 1-(3-hydroxyphenyl)-piperazine; LeuT, leucine transporter; MA, monoamine; NE, norepinephrine; hNET, human norepinephrine transporter; IFD, induced fit docking; PaMLAC, paired mutant–ligand analogue complementation; MD, molecular dynamics; wt, wild-type; POPC, 1-palmitoyl-2-oleoyl-3-sn-phosphatidylcholine; OPLS_2005, optimized potentials for liquid simulations all atom, version 2005

REFERENCES

- (1) Stahl, S. M. (2006) *Essential Psychopharmacology: The Prescriber's Guide. Antipsychotics and Mood Stabilizers*, Cambridge University Press, New York.
- (2) Fischer, J. F., and Cho, A. K. (1979) Chemical release of dopamine from striatal homogenates: evidence for an exchange diffusion model. *J. Pharmacol. Exp. Ther.* 208, 203–209.
- (3) Rudnick, G., and Wall, S. C. (1992) The molecular mechanism of “ecstasy” [3,4-methylenedioxymethamphetamine (MDMA)]: Serotonin transporters are targets for MDMA-induced serotonin release. *Proc. Natl. Acad. Sci. U.S.A.* 89, 1817–1821.
- (4) Ritz, M. C., Lamb, R. J., Goldberg, S. R., and Kuhar, M. J. (1987) Cocaine receptors on dopamine transporters are related to self-administration of cocaine. *Science* 237, 1219–1223.

- (5) Torres, G. E., Gainetdinov, R. R., and Caron, M. G. (2003) Plasma membrane monoamine transporters: Structure, Regulation and Function. *Nat. Rev. Neurosci.* 4, 13–25.
- (6) Giros, B., Jaber, M., Jones, S. R., Wightman, R. M., and Caron, M. G. (1996) Hyperlocomotion and indifference to cocaine and amphetamine in mice lacking the dopamine transporter. *Nature* 379, 606–612.
- (7) Wise, R. A. (1996) Neurobiology of addiction. *Curr. Opin. Neurobiol.* 6, 243–251.
- (8) Chen, R., Tilley, R. C., Wei, H., Zhou, F., Zhou, F. -, Ching, S., Quan, N., Stephens, R. L., Hill, E. R., Nottoli, T., Han, D. D., and Gu, H. H. (2006) Abolished cocaine reward in mice with a cocaine-insensitive dopamine transporter. *Proc. Natl. Acad. Sci. U.S.A.* 103, 9333–9338.
- (9) Beuming, T., Kniazeff, J., Bergmann, M. L., Shi, L., Gracia, L., Raniszewska, K., Newman, A. H., Javitch, J. A., Weinstein, H., Gether, U., and Loland, C. J. (2008) The binding sites for cocaine and dopamine in the dopamine transporter overlap. *Nat. Neurosci.* 11, 780–789.
- (10) Rothman, R. B., Blough, B. E., and Baumann, M. H. (2008) Dual dopamine/serotonin releasers: Potential treatment agents for stimulant addiction. *Exp. Clin. Psychopharmacol.* 16, 458–474.
- (11) Rothman, R. B., Blough, B. E., and Baumann, M. H. (2006) Dual dopamine–5-HT releasers: Potential treatment agents for cocaine addiction. *Trends Pharmacol. Sci.* 27, 612–618.
- (12) Rothman, R. B., Blough, B. E., Woolverton, W. L., Anderson, K. G., Negus, S. S., Mello, N. K., Roth, B. L., and Baumann, M. H. (2005) Development of a rationally designed, low abuse potential, biogenic amine releaser that suppresses cocaine self-administration. *J. Pharmacol. Exp. Ther.* 313, 1361–1369.
- (13) Rothman, R. B., and Baumann, M. H. (2006) Balance between dopamine and serotonin release modulates behavioral effects of amphetamine-type drugs. *Ann. N.Y. Acad. Sci.* 1074, 245–260.
- (14) Gray, D. L., Xu, W., Campbell, B. M., Dounay, A. B., Barta, N., Boroski, S., Denny, L., Evans, L., Stratman, N., and Probert, A. (2009) Discovery and pharmacological characterization of aryl piperazine and piperidine ethers as dual acting norepinephrine reuptake inhibitors and 5-HT1A partial agonists. *Bioorg. Med. Chem. Lett.* 19, 6604–6607.
- (15) Bang-Andersen, B., Ruhland, T., Jørgensen, M., Smith, G., Frederiksen, K., Jensen, K. G., Zhong, H., Nielsen, S. M., Hogg, S., Mørk, A., and Stensbøl, T. B. (2011) Discovery of 1-[2-(2,4-dimethylphenylsulfanyl)phenyl]piperazine (Lu AA21004): A novel multimodal compound for the treatment of major depressive disorder. *J. Med. Chem.* 54, 3206–3221.
- (16) Celik, L., Sinding, S., Severinsen, K., Hansen, C., Møller, M., Bols, M., Wiborg, O., and Schiøtt, B. (2008) Binding of serotonin to the human serotonin transporter. Molecular modeling and experimental validation. *J. Am. Chem. Soc.* 130, 3853–3865.
- (17) Koldsoe, H., Severinsen, K., Tran, T. T., Celik, L., Jensen, H. H., Wiborg, O., Schiøtt, B., and Sinding, S. (2010) The two enantiomers of citalopram bind to the human serotonin transporter in reversed orientations. *J. Am. Chem. Soc.* 132, 1311–1322.
- (18) Sinding, S., Musgaard, M., Jensen, M., Severinsen, K., Celik, L., Koldsoe, H., Meyer, T., Bols, M., Jensen, H. H., Schiøtt, B., and Wiborg, O. (2010) Binding and orientation of tricyclic antidepressants within the central substrate site of the human serotonin transporter. *J. Biol. Chem.* 285, 8363–8374.
- (19) Shenkin, P. S., and McDonald, Q. D. (1994) Cluster analysis of molecular conformations. *J. Comput. Chem.* 15, 899–916.
- (20) (2009) *MacroModel XCluster*, version 9.7, Schrödinger, LLC, New York, NY.
- (21) Boström, J., Norrby, P., and Liljefors, T. (1998) Conformational energy penalties of protein-bound ligands. *J. Comput.-Aided Mol. Des.* 12, 383–383.
- (22) Baker, E. N., and Hubbard, R. E. (1984) Hydrogen bonding in globular proteins. *Prog. Biophys. Mol. Biol.* 44, 97–179.
- (23) Forrest, L. R., Zhang, Y., Jacobs, M. T., Gesmonde, J., Xie, L., Honig, B. H., and Rudnick, G. (2008) Mechanism for alternating access in neurotransmitter transporters. *Proc. Natl. Acad. Sci. U.S.A.* 105, 10338–10343.
- (24) Koldsoe, H., Noer, P., Grouleff, J., Autzen, H. E., Sinding, S., and Schiøtt, B. (2011) Unbiased simulations reveal the inward-facing conformation of the human serotonin transporter and Na⁺ ion release. *PLoS Comput. Biol.* 7, No. e1002246.
- (25) Rothman, R. B., and Baumann, M. H. (2006) Therapeutic potential of monoamine transporter substrates. *Curr. Top. Med. Chem.* 6, 1845–1859.
- (26) Rothman, R. B., Blough, B. E., and Baumann, M. H. (2008) Dopamine/serotonin releasers as medications for stimulant addictions. *Prog. Brain Res.* 172, 385–406.
- (27) Rothman, R., Baumann, M., Dersch, C., Romero, D., Rice, K., Carroll, F., and Partilla, J. (2001) Amphetamine-type central nervous system stimulants release norepinephrine more potently than they release dopamine and serotonin. *Synapse* 39, 32–41.
- (28) Beuming, T., Shi, L., Javitch, J. A., and Weinstein, H. (2006) A comprehensive structure-based alignment of prokaryotic and eukaryotic neurotransmitter/Na⁺ symporters (NSS) aids in the use of the LeuT structure to probe NSS structure and function. *Mol. Pharmacol.* 70, 1630–1642.
- (29) Yamashita, A., Singh, S. K., Kawate, T., Jin, Y., and Gouaux, E. (2005) Crystal structure of a bacterial homologue of Na⁺/Cl⁻-dependent neurotransmitter transporters. *Nature* 437, 215–223.
- (30) Zomot, E., Bendahan, A., Quick, M., Zhao, Y., Javitch, J., and Kanner, B. (2007) Mechanism of chloride interaction with neurotransmitter:sodium symporters. *Nature* 449, 726–730.
- (31) Forrest, L. R., Tavoulari, S., Zhang, Y. W., Rudnick, G., and Honig, B. (2007) Identification of a chloride ion binding site in Na⁺/Cl⁻-dependent transporters. *Proc. Natl. Acad. Sci. U.S.A.* 104, 12761–12766.
- (32) Schrödinger L.L.C. (2006) Schrödinger Suite 2006, Maestro version 7.5, MacroModel version 9.1, Glide version 4.0, Prime version 1.5.
- (33) Polak, E., and Ribiere, G. (1969) Note on convergence of conjugate direction methods. *Rev. Fr. Inform. Rech. Oper.* 3, 35–43.
- (34) Halgren, T. A. (1996) Merck molecular force field: I. Basis, form, scope, parameterization and performance of MMFF94. *J. Comput. Chem.* 17, 490–519.
- (35) (2005) Schrödinger Suite 2006 Induced Fit Docking protocol; Glide version 4.0, Schrödinger, LLC, New York, NY; (2005) Prime version 1.5, Schrödinger, LLC, New York, NY.
- (36) Sherman, W., Day, T., Jacobson, M. P., Friesner, R. A., and Farid, R. (2006) Novel procedure for modeling ligand/receptor induced fit effects. *J. Med. Chem.* 49, 534–553.
- (37) Friesner, R. A., Banks, J. L., Murphy, R. B., Halgren, T. A., Klicic, J. J., Mainz, D. T., Repasky, M. P., Knoll, E. H., Shelley, M., Perry, J. K., Shaw, D. E., Francis, P., and Shenkin, P. S. (2004) Glide: A new approach for rapid, accurate docking and scoring. 1. Method and assessment of docking accuracy. *J. Med. Chem.* 47, 1739–1749.
- (38) Friesner, R. A., Murphy, R. B., Repasky, M. P., Frye, L. L., Greenwood, J. R., Halgren, T. A., Sanschagrin, P. C., and Mainz, D. T. (2006) Extra Precision Glide: Docking and scoring incorporating a model of hydrophobic enclosure for protein-ligand complexes. *J. Med. Chem.* 49, 6177–6196.
- (39) Still, W. C., Tempczyk, A., Hawley, R. C., and Hendrickson, T. (1990) Semianalytical treatment of solvation for molecular mechanics and dynamics. *J. Am. Chem. Soc.* 112, 6127–6129.
- (40) (2008) MacroModel, version 9.6, Schrödinger, LLC, New York, NY.
- (41) Jorgensen, W. L., Maxwell, D. S., and Tirado-Rives, J. (1996) Development and Testing of the OPLS All-Atom Force Field on Conformational Energetics and Properties of Organic Liquids. *J. Am. Chem. Soc.* 118, 11225–11236.
- (42) Kaminski, G. A., Friesner, R. A., Tirado-Rives, J., and Jorgensen, W. L. (2001) Evaluation and reparametrization of the OPLS-AA force field for proteins via comparison with accurate quantum chemical calculations on peptides. *J. Phys. Chem. B* 105, 6474–6487.

- (43) (2008) Desmond Molecular Dynamics System, version 2.0, D. E. Shaw Research, New York, NY.
- (44) (2008) Maestro-Desmond Interoperability Tools, version 2.0, Schrödinger, New York.
- (45) Bowers, K. J., Chow, E., Xu, H., Dror, R. O., Eastwood, M. P., Gregersen, B. A., Klepeis, J. L., Kolossvary, I., Moraes, M. A., Sacerdoti, F. D., Salmon, J. K., Shan, Y., and Shaw, D. E. (2006) *Scalable algorithms for molecular dynamics simulations on commodity clusters*, ACM: New York, Tampa, FL.
- (46) Jorgensen, W. L., Chandrasekhar, J., Madura, J. D., Impey, R. W., and Klein, M. L. (1983) Comparison of simple potential functions for simulating liquid water. *J. Chem. Phys.* 79, 926–935.
- (47) Weinbach, Y., and Elber, R. (2005) Revisiting and parallelizing SHAKE. *J. Comput. Phys.* 209, 193–206.
- (48) Berendsen, H. J. C., Postma, J. P., van Gunsteren, W. F., DiNola, A., and Haak, J. R. (1984) Molecular dynamics with coupling to an external bath. *J. Chem. Phys.* 81, 3684–3690.
- (49) Essmann, U., Perera, L., Berkowitz, M. L., Darden, T., Lee, H., and Pedersen, L. G. (1995) A smooth particle mesh Ewald method. *J. Chem. Phys.* 103, 8577–8593.
- (50) Ewald, P. P. (1921) Die Berechnung optischer und elektrostatischer Gitterpotentiale. *Ann. Phys.* 64, 253–287.
- (51) Pariser, J. J., Partilla, J. S., Dersch, C. M., Ananthan, S., and Rothman, R. B. (2008) Studies of the biogenic amine transporters. 12. Identification of novel partial inhibitors of amphetamine-induced dopamine release. *J. Pharmacol. Exp. Ther.* 326, 286–295.
- (52) Rothman, R. B., Vu, N., Partilla, J. S., Roth, B. L., Huiseisen, S. J., Compton-Toth, B. A., Birkes, J., Young, R., and Glennon, R. A. (2003) In vitro characterization of ephedrine-related stereoisomers at biogenic amine transporters and the receptorome reveals selective actions as norepinephrine transporter substrates. *J. Pharmacol. Exp. Ther.* 307, 138–145.
- (53) Nightingale, B., Dersch, C. M., Boos, T. L., Greiner, E., Calhoun, W. J., Jacobson, A. E., Rice, K. C., and Rothman, R. B. (2005) Studies of the biogenic amine transporters. XI. Identification of a 1-[2-[bis(4-fluorophenyl)methoxy]ethyl]-4-(3-phenylpropyl)piperazine (GBR12909) analog that allosterically modulates the serotonin transporter. *J. Pharmacol. Exp. Ther.* 314, 906–915.